Superparamagnetic Nanocomposite of Magnetite-Chitosan Using Oleic Acid as Anti Agglomeration and Glutaraldehyde as Crosslinkage Agent

Suyanta[*], Sutarno, Nuryono, Bambang Rusdiarso, Eko Sri Kunarti, Hesti Kusumastuti, and Lia Kurnia

*Department of Chemistry, Faculty of Mathematics and Natural Sciences, Universitas Gadjah Mada,
Sekip Utara, Yogyakarta 55281, Indonesia*

Abstract: *In this research magnetite was synthesized by coprecipitation method, in which solution of NH₄OH was added into the solution containing a mixture of Fe^{2+}/Fe^{3+} (molar ratio 1:2) until pH 11 under strong ultrasonic agitation for 30 min. The black sediment of magnetite was filtered, washed and dried. The product was then modified by using oleic acid to prevent agglomeration. Chitosan was prepared by deacetilization of chitin, whereas chitin was extracted from shrimp shell. In the synthesis of nanocomposite, 0.5 g of chitosan and 1.5 g of oleic acid modified magnetite were introduced into 100 mL of 2% acetic acid solution, followed by sonication treatment for 10 min and magnetic stirring for 20 min. In order to perform the cross-linkage reaction, solution of 2% glutaraldehyde was added into the mixture at temperature of 40 °C for 3 h. The composite was collected by magnetic separation, followed by washing with distilled water and ethanol in a row. The product was dried and characterized by XRD, FTIR, TEM and VSM methods. The result showed that the composite had good crystal structure with a cubic inverse spinel structure, monodisperse and quasi sphere in shape with diameter of 20–25 nm. It had high saturation magnetization (43.4 emu/g) and superparamagnetic property.*

Keywords: *nanocomposite; magnetite; oleic acid; chitosan*

■ INTRODUCTION

Chitosan is a linear copolymer of linked β-(1,4)-glucosamine molecules, mainly obtained by deacetylation of chitin (poly-β-(1,4)-acetylglucosamine); whereas chitin can be obtained from wastes of the seafood industry (crab and shrimp shells) involves some steps, i.e.: demineralization, deproteinization, and decolorization [1-2]. Chitosan can be used in water treatment, especially heavy metals, because the functional groups of –NH₂ in the glucose ring react strongly with metal ions in a large capacity [3]. It has high porosity resulting in superior binding properties for metal ion such as cadmium, copper, lead, uranyl, mercury and chromium [4-8]. However, some weakness related to their poor chemical and mechanical stability caused it low in effectiveness and efficiency when were applied as adsorbent in the industrial scale.

One of many ideas to overcome these problem is the compositazion by using magnetite (Fe_3O_4). This treatment leads to had better performance due to the increasing specific surface area and to the possibility to remove the used adsorbent from the contaminated waste streams by an external magnetic field in order to regenerate it for subsequent reuse [9-10].

Magnetite Nanoparticles (MNPs) has a large surface area and high affinity toward metal ions; however it tend to agglomerate lead a bulk phase which has lower in performance. Fortunately, those agglomeration can be prevented by coating with various hydrophilic compounds. Oleic acid (OA) is probably the most common small molecule which can formed the complex with magnetite [11]. OA possesses a non-polar hydrocarbon tail and a polar carboxylic acid head group. Carboxylate anions are known to coordinate with the

surface of magnetite, presumably through a coordination of iron atoms with both the carboxylate oxygens [12].

Compositazion of chitosan with modified MNPs favor the generation of hydrogen bonding between positively partial charged hydrogen of chitosan and negatively partial charged oxygen of Fe_3O_4, thus improve their interfacial combination [13]. On the other hand cross-linking reaction can significantly alter the molecular structure of materials, therefore the properties of cross-linked materials could significantly differ from those of the original materials.

In this work, chitosan was extracted from shrimp shell, while magnetite was synthesized and modified by using oleic acid to prevent agglomeration and get the nano scale. Chitosan was then interacted with nanoparticle magnetite to obtain a nanocomposite in which chitosan has higher surface area, moreover the material can be quickly separated using external magnetic field. Finally, nanocomposite particles were cross-linkage by using glutaraldehyde to improve the stability.

■ EXPERIMENTAL SECTION

Materials

Iron(III) chloride hexahydrate ($FeCl_3 \cdot 6H_2O$), iron(II) sulfate heptahydrate ($FeSO_4 \cdot 7H_2O$), aqueous ammonia (25%), glutaraldehyde, acetic acid, and ethanol. All of materials were purchased from E. Merck, All chemicals are analytical grade without further purification. Shrimp shell was gained from a local culinary. Distilled water was used throughout the experiments.

Instrumentation

Infrared spectrophotometer Shimadzu FTIR-8010PC, X-ray Diffractometer Shimadzu model XD-3H, Transmission Electron Microscope JEM-3010, Vibrating Sample Magnetometer (VSM Oxford 1.2H), Ultrasonic 28H, and some support instruments.

Procedure

Preparation of chitosan

Preparation of chitosan from shrimp shells was performed using the method used by Kusumaningrum [14] and Kurnia [15], include: deproteination,

demineralization, decolorization and deacetylation. In the deproteination step, 50 g of raw shrimp shells were introduced into 500 mL of 1 M NaOH solution accompanied by stirring at 65 °C for 60 min. It was then filtered, the solid phase was washed and dried. The product was demineralized by took into solution of 1 M HCl (with proportion 1 g of solid phase in 15 mL of HCl solution) followed by stirring at 80 °C for 90 min. Filtering of those mixture produced the solid of chitin. In order to omit the color, chitin was bleached by using solution of 4% NaOCl (with proportion 1 g of chitin in 10 mL of NaOCl solution) at room temperature for 60 min, furthered by filtering. The solid phase was deacetylized by put into solution of NaOH 60% w/w, followed by stirring at 90 °C for 2 h formed a slurry. The slurry was then filtered, washed and dried to produce the powder of chitosan.

The samples of chitosan produced from varied w/w % of NaOH were characterized using Fourier Transform Infrared (FTIR) spectrophotometer in the range of 400 to 4000 cm^{-1}. The DDA of the sample were determined according to the method which was generally used. The A1320 was the peak area of the band about 1320 cm^{-1}, the A1420 was the peak area of about 1420 cm^{-1} and A(1320) is peak for amide group and A(1420) is peak for amine group.

$$\%DA = \frac{\left(A1320 / A1420 \right) - 0.3822}{0.03133} \qquad (1)$$

$$\%DDA = 100 - \%DA \qquad (2)$$

where, DDA = degree of deacetylation (%) and DA = degree of acetylation (%).

Preparation of Fe_3O_4 nanoparticles

Fe_3O_4 nanoparticles were prepared by coprecipitation method with a ferrous complex in presence of NH_4OH. First, $FeCl_2 \cdot 4H_2O$ and $FeCl_3 \cdot 6H_2O$ [$Fe^{2+}:Fe^{3+}$ = 1:2] were dissolved in 50 mL distilled water. The solution was stirred under strong ultrasonic agitation accompanied by heating at 80 °C. Next, the solution of 3 M NH_4OH was added drop-wise into those iron solution source until pH 11 under strong ultrasonic agitation for 30 min. The black deposit of Fe_3O_4 nanoparticles were separated by filtering and washed by distilled water three times.

Surface modification of magnetite nanoparticles with oleic acid

The magnetite nanoparticles were well dispersed in 200 mL of methanol by ultrasonication. It was then added with 50 mL of oleic acid accompanied by constant stirring at 80 °C. Nanoparticles of magnetite-oleic acid were filtered through Whatman filter paper no.1, followed by washing three times with distilled water. The magnetite-oleic acid nanoparticles were separated from the filter paper using acetone, followed by drying at room temperature to evaporate all the acetone. These materials were termed as Fe_3O_4-OA NPs.

Preparation of magnetite-chitosan nanocomposite

Chitosan (0.5 g) in 100 mL of 2.0 wt.% acetic acid solution was mixed with 1.5 g of Fe_3O_4-OA NPs in a three-necked flask. The mixture was treated with ultrasonic for 10 min and stirred for 20 min. Then 2 mL of glutaraldehyde solution (25 wt.%) was added into the mixture at 40 °C and crosslinking reaction was kept for 3 h. After the reaction the composites were collected through magnetic separation and were washed by distilled water and ethanol for three times. The products were dried at vacuum conditions.

■ RESULTS AND DISCUSSION

Characterization of Chitosan

The FTIR spectra of shrimp shells powder, chitin and chitosan were presented in Fig. 1. The shrimp shells powder's spectrum (Fig. 1(a)) exhibited some bands at wave number 3449, 1651, and 1072 cm^{-1}; the chitin spectrum (Fig. 1(b)) showed some new bands at wave number 3264, 3109, 2886, and 1072 cm^{-1} accompanied by little displacement of band from 1651 to 1628 cm^{-1}; while chitosan spectrum (Fig. 1(c)) in brief displayed the new four bands at 1659, 1589, 1421, and 1072 cm^{-1} accompanied by the absence of band at 3264 cm^{-1} which was appeared on chitin spectrum. Those differences indicated that alteration of bonds in the materials have been occurred, from shrimp shells to chitin and from chitin to chitosan.

The absorption bands at 3449 cm^{-1} which appeared on all materials spectra is due to overlapping of the OH and N-H stretching vibration of functional groups engaged
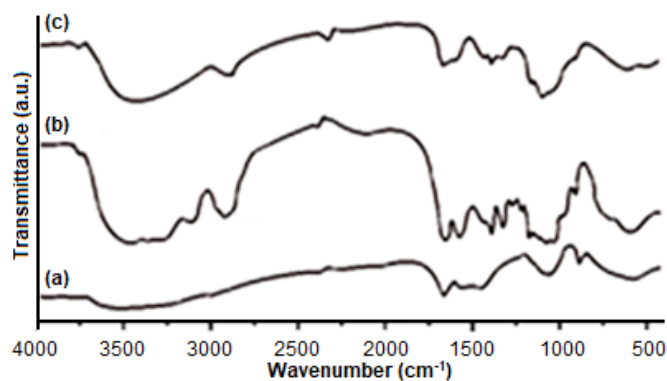

Fig 1. The FTIR spectra of shrimp shells powder (a), chitin (b) and chitosan (c) [14-15]

in hydrogen bond [16]. The bands at 3264 and 3109 cm^{-1} which appeared on chitin spectrum only related to vibrational modes involved in intermolecular hydrogen bonding CO• • •HN and the intramolecular bonds of NH groups, respectively [17]. The bands at 2886 cm^{-1} which appeared on both of chitin and chitosan spectra is due to symmetric and asymmetric –CH$_2$– vibration attributed to pyranose ring [18].

The two separate bands at 1659 and 1589 cm^{-1} on chitosan spectrum are due to -C=O stretching (amide I) and NH stretching (amide II) [19]. In the case of both chitin and shrimp shells powder, a single peak at 1627 or 1651 cm^{-1} corresponds to the stretching of CO group intra-sheet chain and also showing the presence of protein [20-21]. The absorption bands from 1100 to 1020 cm^{-1} (included 1072 cm^{-1}) which appeared on all materials spectra come from the C–O–C and C–O stretching vibrations of the structure [22]. The other bands that are observed in the region of 1380–1460 cm^{-1} are attributed to the symmetric and asymmetric bending vibrations of the methyl groups [23].

The DDA in this work is large enough (86.88%), indicating the good efficiency for this process in this established condition. Those value is also very near to that reported by some researchers. Al Sagheer et al. [15] reported that the chitosan DDA obtained from shrimp shell waste in Arabian Gulf ranged from 88–94% by using traditional method. Nouri et al. [24] also obtained DDA value ranged from 71.02–82.20% for deacetylation using traditional method while 79.01–88.60% for using microwave method. Besides, Alishahi et al. [25] also performed deacetylation by using microwave and obtained chitosan with DDA value ranged from 87.5–93%.
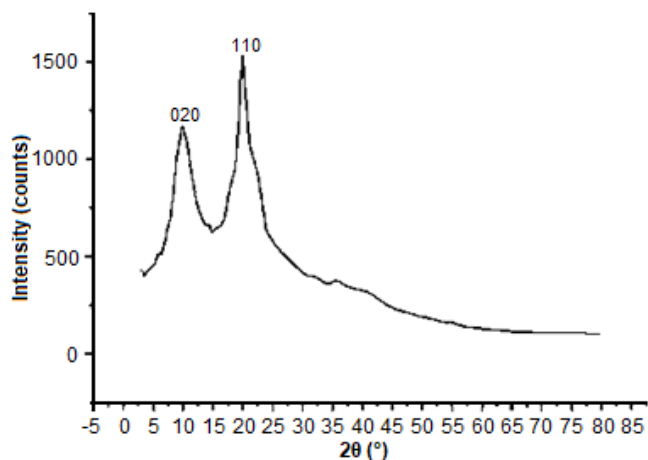
Fig 2. The XRD pattern for chitosan [14-15]

Fig 3. XRD patterns of the pristine Fe_3O_4 (a), and Fe_3O_4 MNPs coated with 1, 2 and 3 mL of OA in modification (b, c, and d) [14-15]

XRD analysis is based on constructive interference of monochromatic X-rays. It is a non-destructive technique widely used to investigate the interlayer changes and the crystalline properties of the synthesized material. The inter-planer distances may be calculated by the following Braggs'equation.

$$n\lambda = 2d_{hkl}\sin\theta \qquad (3)$$

where λ is the wavelength of the X-ray, θ is the scattering angle, n is an integer representing the order of the diffraction peak, d is the inter planer distance of the lattices, and (hkl) are the Miller indices [18].

The obtained XRD pattern for chitosan measured in the range of $2\theta = 10\text{-}40°$ (Fig. 2) showed two characteristic reflections at 9.93 and 19.98° that are typical fingerprints of semi crystalline chitosan indexed as (020) and (110) known as hydrated crystalline structure and an amorphous structure of chitosan [26]. Yen and Mau [27] found that fungal chitosan showed two crystalline reflections at 9.7 and 19.9°. This is caused by presence of plenty of –OH and –NH$_2$ groups in the chitosan structure, which could form stronger inter and intramolecular hydrogen bonds and the chitosan structure has certain regularity, so that the molecules form crystalline regions easily. It is also reported that the two characteristic crystalline peaks with slightly fluctuated diffraction angles found in the wide-angle X-ray diffraction (WAXD) patterns indicated that two types of α- and γ-chitosan exhibited comparable degree of crystallinity and had two consistent peaks of 9–10° and 19–20° [28].
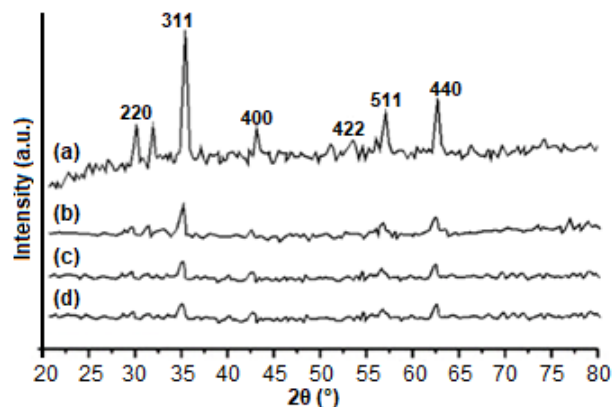
Characterization of Magnetite and Oleic Acid Modified Magnetite

Fig. 3 shows the XRD patterns of the pristine Fe_3O_4 (a), and Fe_3O_4 MNPs coated with varied volume of OA (b-d). The peaks at $2\theta = 30.1, 35.4, 43.1, 53.4, 56.9,$ and 62.5°, corresponding to 220, 311, 400, 422, 511, and 440 Bragg reflection planes, which were observed in all of the samples. These peaks are consistent with the standard pattern of Fe_3O_4 (JCPDS no. 79-0418) with a cubic inverse spinel structure [29]. Therefore, it was confirmed that the crystalline structure of obtained magnetite nanoparticles, agreed with the structure of an inverse spinel type oxide. The presence of peaks in all of the samples indicated that the crystal structure of Fe_3O_4 NPs was not changed during the modification with oleic acid.

The capping of Fe_3O_4 with OA caused the broadening of peaks accompanied by descent of its intensity proportional to volume of OA added. It indicated that the particle size decreased after coating treatment. The coating of amorphous OA on crystalline Fe_3O_4 may induce microstrain which resulted in broadening of peaks also were reported by some researchers [30-31]. The crystallite size of oleic acid modified Fe_3O_4 NPs smaller than the pristine one, indicated that the aim of oleic acid modification has achieved. The diffractogram of sample coated with 3 mL of OA (Fig. 4(d)) has smallest peaks, indicating the most complete coating; therefore the sample was choose for the next treatment.
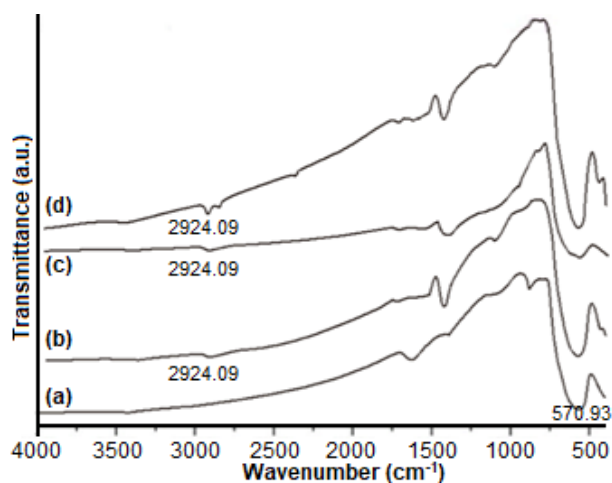
Fig 4. FTIR spectra of the pristine Fe_3O_4 (a), and Fe_3O_4 MNPs coated with 1, 2 and 3 mL of OA in modification (b, c, and d) [14-15]

Fig 5. FT-IR spectra of pristine Fe_3O_4 NPs (a), oleic acid modified Fe_3O_4 NPs (b) and Fe_3O_4-chitosan nanocomposite (c) [14-15]

Fig. 4 shows the typical FTIR spectrum of the pristine Fe_3O_4 nanoparticles (a), and Fe_3O_4 nanoparticles coated with varied volume of oleic acid (b-d). Spectrum (a) has a sharp band only at 570 cm⁻¹ corresponding to the Fe–O vibration related to the magnetite phase [32], whereas the others have two extra bands at 2924 and 2854 cm⁻¹ which attributed to the asymmetric CH_2 stretch and the symmetric CH_2 stretch, respectively. These extra band more and more clear when volume of OA added increased. In addition to the new bands at about 1500 and 1600 cm⁻¹ which characteristic of the asymmetric and symmetric stretching of COO– group, respectively. This result proved that the bonding pattern of the carboxylic acids on the surface of Fe_3O_4 nanoparticles was a combination of molecules bonded symmetrically and molecules bonded at an angle to the surface [33].

Fig. 5 shows the FT-IR spectrum of pristine Fe_3O_4 NPs (a), oleic acid modified Fe_3O_4 NPs (b) and Fe_3O_4-oleic acid-chitosan composite (c). The characteristic peaks of Fe_3O_4 at about 570 cm⁻¹ could be seen in all of the three spectra which indicated the presence of Fe_3O_4. The peaks at around 3448 and 1630 cm⁻¹ in all of them are related to the adsorbed water in the samples. The characteristic peaks of oleic acid can be observed at 2924 and 2854 cm⁻¹ in curve (b) and (c) which related to the symmetric and asymmetric stretch of CH_3 and CH_2. The peaks at around 1600 and 1400 cm⁻¹ in curve (b) and (c) due to the
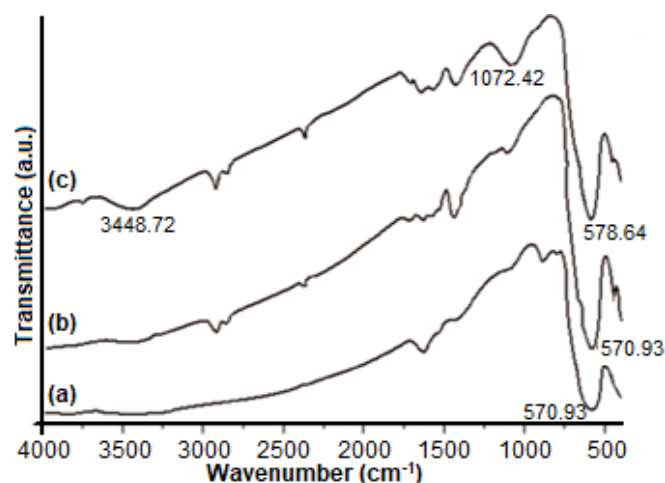
asymmetric and symmetric stretching band of COO⁻ of oleate [34-35]. The absorption peak near 1110 cm⁻¹ in curve (b) and (c) can be ascribed to the vibration of O–C–O bond of the oleate. These results indicated that the oleic acid has changed into oleate and coated onto the surface of the Fe_3O_4 NPs. The new peak appears at 1627 cm⁻¹ (overlap with other band) come from imine groups, (N=C) produced by reaction between chitosan with glutaraldehyde [35]. While the shifting of Fe_3O_4 characteristic peaks from 571 cm⁻¹ (Fig. 5(a)) to 579 cm⁻¹ (Fig. 5(b)) indicated possible binding of irons from magnetite to NH_2 as well as -OH groups of chitosan. In addition, electrostatic interaction between surface negative charged Fe_3O_4 and positively protonated chitosan can also contribute [36].

Based on those explanation, it can be predicted that chitosan has been coated on the oleic acid modified Fe_3O_4 nanoparticle successfully. The interaction model was presented on Fig. 6, which to consist of three steps. In the first step, the molecules of oleic acid prevent aglomeration of magnetite particles. In the second step, chitosan molecules interact with nanoparticles of mgnetite-oleic acid via both of –NH_2 and –OH group. While in the third step, glutaraldehyde molecules crosslink the chitosan molecules which have interacted with nanoparticles of magnetite-oleic acid.
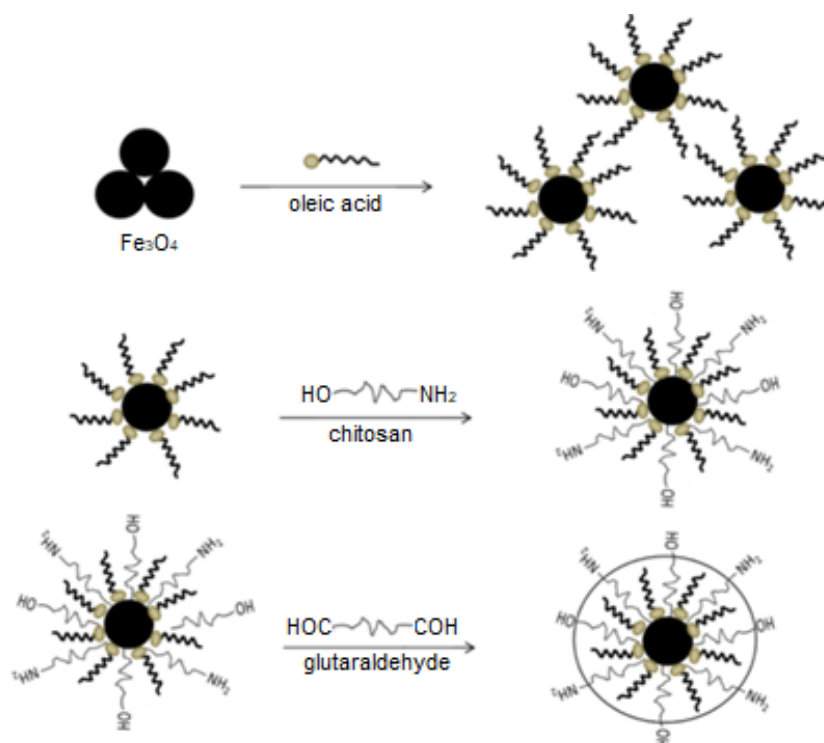
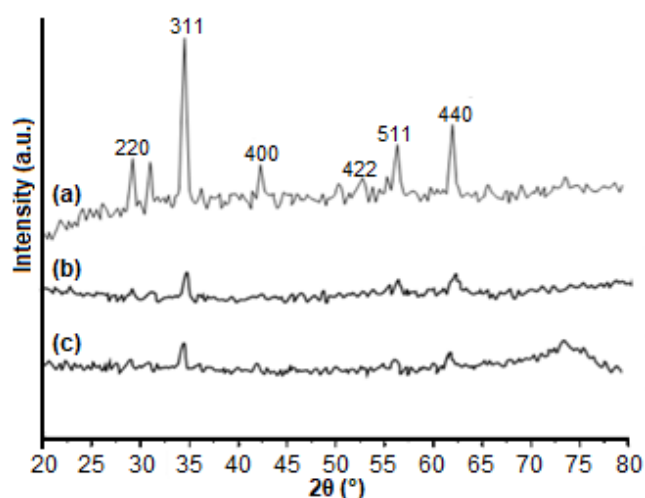**Fig 6.** Interaction model in the formation of the nanocomposite

Fig 7. XRD patterns of pristine Fe₃O₄ NPs (a), oleic acid modified Fe₃O₄ NPs (b) and the nanocomposite of Fe₃O₄-chitosan (c) [14-15]

Fig 8. Room temperature magnetization curves for pristine Fe₃O₄ (a), oleic acid modified Fe₃O₄ NPs (b) and Fe₃O₄–chitosan nanocomposite (c) [14-15]

Characterization of Nanocomposite

Fig. 7 exhibits the XRD patterns comparation of pristine Fe_3O_4 NPs (a), oleic acid modified Fe_3O_4 NPs in optimal condition (b) and nanocomposite of Fe_3O_4-chitosan (c). There are 6 of characteristic peaks for Fe_3O_4
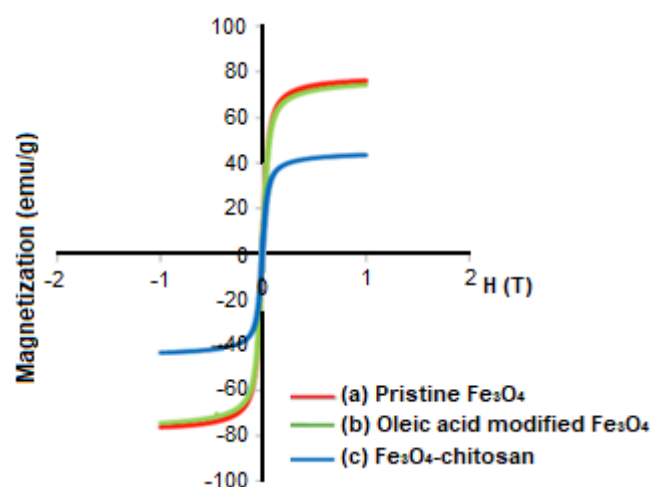
(2θ = 30.1, 35.4, 43.1, 53.4, 56.9, and 62.5°) were observed in all of the samples.

These peaks are consistent with the standard pattern for Fe_3O_4 (JCPDS no. 79-0418) with a cubic inverse spinel structure. The Quite weak diffraction lines of composite patterns (Fig. 7(c)) indicated that Fe_3O_4 particles
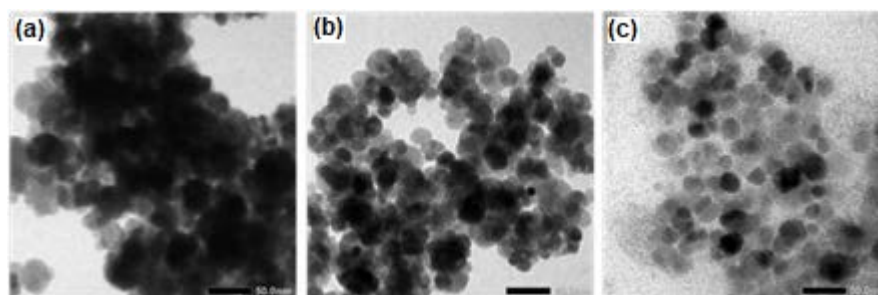
Fig 9. TEM images of pristine Fe_3O_4 (a), oleic acid modified Fe_3O_4 (b) and Fe_3O_4–chitosan nanocomposite (c) [14-15]

have been coated by amorphous chitosan. It is parallel with interpretation of FTIR spectra. Furthermore, this coating did not change the phase of Fe_3O_4. The results showed that the modification did not change the crystal structure of the Fe_3O_4 NPs.

The mean crystal sizes were determined by the Debye–Scherrer equation with XRD data, $D = K\lambda/(\beta\cos\theta)$, where K is a constant (K = 0.94 for Cu-Kα), λ is the wavelength (0.15405 nm for Cu-Kα), β the full-width at half maximum (FWHM) of the strongest reflection of the (311) peak, and θ is the diffraction angle [37]. Based on those equation, the crystal sizes of pristine Fe_3O_4, oleic acid modified Fe_3O_4 NPs and Fe_3O_4 NPs in the nanocomposite of Fe_3O_4–chitosan were found to be approximately 23, 14, and 13 nm respectively.

Magnetic properties of Fe_3O_4, oleic acid modified Fe_3O_4 and nanocomposite of Fe_3O_4–chitosan were characterized by vibrating sample magnetometer (VSM). The magnetic hysteresis curves are shown in Fig. 8, (a) pristine Fe_3O_4 NPs (b) oleic acid modified Fe_3O_4 NPs and (c) Nanocomposite of Fe_3O_4–chitosan.

It can be seen that no coercivity or remanence could be observed for all of the three samples, suggesting the superparamagnetic properties of the Fe_3O_4 NPs. This can be ascribed to the small size of NPs which were smaller than the superparamagnetic critical size (25 nm) [38]. The saturation magnetization of pristine Fe_3O_4, oleic acid modified Fe_3O_4 NPs and nanocomposite of Fe_3O_4–chitosan were 76.0, 74.0 and 43.4 emu/g respectively. The high saturation magnetization of pristine Fe_3O_4 and oleic acid modified Fe_3O_4 NPs indicated the good crystal structure. There is no large difference in saturation magnetization between them, because the layer of oleic acid is slight only. On the other hand, saturation

magnetization of Fe_3O_4–chitosan nanocomposite was much lower than that of the pristine Fe_3O_4. This was due to the existence of the large amount of diamagnetic chitosan in the Fe_3O_4–chitosan NPs [38]. Although, the values of the saturation magnetization of this work were much larger than the result reported in the literature (22 emu/g) [39].

Fig. 9 shows the TEM images of pristine Fe_3O_4, oleic acid modified Fe_3O_4, and Fe_3O_4–chitosan nanocomposite. It is clear that pristine Fe_3O_4 were quite agglomerated, while oleic acid modified Fe_3O_4 and Fe_3O_4–chitosan nanocomposite particles was looser, less agglomerated, and uniform in particle size. Image of c showed that Fe_3O_4–chitosan nanocomposite particles were quasi-spherical and had good dispersity.

The size of Fe_3O_4–chitosan nanocomposite particles were 20–25 nm, while of Fe_3O_4 particles in the Fe_3O_4–chitosan nanocomposite were about 14 nm which is close to the calculation using the Debye–Scherrer equation in the XRD data. Those images also exhibited the formation of the Fe_3O_4–chitosan nanoparticles with core-shell structure which has a different contrasts. The dark areas represent crystalline Fe_3O_4, while the bright ones are assigned for amorphous chitosan. In addition, a slight aggregation can be seen which was caused by the crosslinking between the different nanoparticles.

■ CONCLUSION

The as-synthesized Fe_3O_4–chitosan nanocomposite had good crystal structure with a cubic inverse spinel structure, monodisperse and quite sphere in shape with diameter of 20–25 nm. The particle size of Fe_3O_4 in the nanocomposite was about 14 nm with narrow in size distribution. The Fe_3O_4–chitosan nanocomposite

exhibited high saturation magnetization (43.4 emu/g) and superparamagnetic property. There are interaction between Fe_3O_4 nanoparticles and chitosan in which irons from magnetite interact with $-NH_2$ as well as $-OH$ groups of chitosan. Additionally, electrostatic interaction between surface negative charged Fe_3O_4 and positively protonated chitosan can also contribute.

■ **ACKNOWLEDGMENTS**

■ **REFERENCES**

[1] Futalan, C.M., Khan, C.C., Dalida, M.L.P., Pascua, C., Hsien, K.J., and Wan, M.W., 2011, Nickel removal from aqueous solution in fixed bed Using chitosan coated bentonite, *Sustainable Environ. Res.*, 21 (6), 361–367.

[2] Ramya, R., Sankar, P., Anbalagan, S., and Sudha, P.N., 2011, Adsorption of Cu(II) and Ni(II) ions solutions using crosslinked chitosan polymer, *Int. J Environ. Sci.*, 1 (6), 1323–1338

[3] Divakaran, R., Paul, A., Anoop, A.J., Kuriakose, K.K.A., and Rajesh, V.J.R., 2012, Adsorption of nickel(II) and chromium(VI) ions by chitin and chitosan from aqueous solutions containing Both ions, *Int. J. Sci. Technol. Res.*, 1, 43–50.

[4] Zheng, W., Li, X.M., Yang, Q., Zeng, G.M., Shen, X.X., Zhang, J., and Liu, J.J., 2007, Adsorption of Cd(II) and Cu(II) from aqueous solution by carbonate hydroxyapatite derived from egg shell waste, *J. Hazard. Mater.*, 147 (1-2), 534–539.

[5] Yan, H., Yang, L., Yang, Z., Yang, H., Li, A., and Cheng, R., 2012, Preparation of chitosan/poly(acrylic acid) magnetic composite microspheres and applications in the removal of copper(II) ions from aqueous solutions, *J. Hazard. Mater.*, 229-230, 371–380.

[6] Akkaya, R., and Ulusoy, U., 2008, Adsorptive features of chitosan entrapped in polyacrylamide hydrogel for Pb^{2+}, UO_2^{2+}, and Th^{4+}, *J. Hazard. Mater.*, 151 (2-3), 380–388.

[7] Kushwaha, S., and Sudhakar, P.P., 2011, Adsorption of mercury(II), methyl mercury(II) and phenyl mercury(II) on chitosan crosslinked with a barbital derivative, *Carbohydr. Polym.*, 86 (2), 1055–1062.

[8] Wen, Y., Tang, Z., Chen, Y, and Gu, Y., 2011, Adsorption of Cr(VI) from aqueous solutions using chitosan-coated fly ash composite as biosorbent, *Chem. Eng. J.*, 175, 110–116.

[9] Ambashta, R.D., and Sillanpaa, M., 2010, Water purification using magnetic assistance: A review, *J. Hazard. Mater.*, 180 (1-3), 38–49.

[10] Petrova, T.M., Fachikov, L., and Hristov, J., 2011, The magnetite as adsorbent for some hazardous species from aqueous solutions: A review, *Int., Rev. Chem. Eng.*, 3, 134–152.

[11] Zureick, A.H., Shih, B., and Munley, E., 1995, Fiber-reinforced polymeric bridge decks, *Struct. Eng. Rev.*, 7 (3), 257–266.

[12] Shete, P.B., Patil, R.M., Tiwale, B.M., and Pawar, S.H., 2015, Water dispersible oleic acid-coated Fe_3O_4 nanoparticles for biomedical applications, *J. Magn. Magn. Mater.*, 377, 406–410.

[13] Patil, R.M., Shete, P.B., Thorat, N.D., Otari, S.V., Barick, K.C., Prasad, A.I., Ningthoujam, R.S., Tiwale, B.M., Pawar, S.H., 2014, Non-aqueous to aqueous phase transfer of oleic acid coated iron oxide nanoparticles for hyperthermia application, *RSC Adv.*, 4 (9), 4515–4522.

[14] Kusumaningrum, H., 2016, Sintesis Komposit Kitosan-Magnetit Termodifikasi Asam Oleat dan Kajian Kelayakannya sebagai Adsorben Hg(II), *Undergraduate Thesis*, Department of Chemistry, Universitas Gadjah Mada, Yogyakarta.

[15] Kurnia, L., 2016, Sintesis Komposit Kitosan-Magnetit Termodifikasi Asam Oleat dan Aplikasinya sebagai Adsorben Cr(III) dalam Larutan Berair, *Undergraduate Thesis*, Department of Chemistry, Universitas Gadjah Mada, Yogyakarta.

[16] Kumar, N.S., Suguna, M., Subbaiah, M.V., Reddy, A.S., Kumar, N.P., and Krishnaiah, 2010, Adsorption of phenolic compounds from aqueous

solution onto chitosan-coated perlite beads as biosorbent, *Ind. Eng. Chem. Res.*, 49 (19), 9238–9247.

[17] Kumari, S., Rath, P., and Kumar, A.S.H., 2016, Chitosan from shrimp shell (*Crangon crangon*) and fish scales (*Labeorohita*): Extraction and characterization, *Afr. J. Biotechnol.*, 15 (24), 1258–1268.

[18] Soni, U., Bajpai, J., and Bajpai, A.K., 2015, Chitosan-activated carbon nanocomposites as potential biosorbent for removal of nitrophenol from aqueous solutions, *Int. J. Nanomater. Biostruct.*, 5 (4), 53–61.

[19] Kweon, H.Y., Um, I.C., and Park, Y.H., 2001, Structural and thermal characteristics of *Antheraea pernyi* silk fibroin/chitosan blend film, *Polymer*, 42 (15), 6651–6656.

[20] Hajji, S., Younes, I., Ghorbel-Bellaa, O., Hajji, R., Rinaudo, M., Nasri, M., and Jellouli, K., 2014, Structural differences between chitin and chitosan extracted from three different marine sources, *Int. J. Biol. Macromol.*, 65, 298–306.

[21] Chouwatat, P., Polsana, P., Noknoi, P., Siralertmukul, K., and Srikulkit, K., 2010, Preparation of hydrophobic chitosan using complexation method for PLA/chitosan blend, *J. Met. Mater. Miner.*, 20 (1), 41–44.

[22] Choi, C.Y., Kim, S.B., Pak, P.K., Yoo, D.I., and Chung, Y.S., 2007, Effect of *N*-acylation on structure and properties of chitosan fibers, *Carbohydr. Polym.*, 68 (1), 122–127.

[23] Li, Q., Weng, S., Wu, J., and Zhou, N., 1998, Comparative study on structure of solubilized water in reversed micelles. 1. FT-IR spectroscopic evidence of water/AOT/*n*-heptane and water/NaDEHP/*n*-heptane systems, *J. Phys. Chem. B*, 102 (17), 3168–3174.

[24] Nouri, M., Khodaiyan, F., Razavi, S.H., and Mousavi, M., 2016, Improvement of chitosan production from Persian Gulf shrimp waste by response surface technology, *Food Hydrocolloids*, 59, 50-58.

[25] Alishahi, A., Mirvaghefi, A., Tehrani, M.R., Farahmunh, H., Shojaosadati, S.A., Dorkoosh, F.A., and Maher, Z.E., 2011, Enhancement and characterization of chitosan extraction from the wastes of shrimp packaging plants, *J. Polym. Environ.*, 19 (3), 776–783.

[26] Yen, M.T., and Mau, J.L., 2007, Physico-Chemical Characterization of fungal chitosan from shiitake stipes, *LWT Food Sci. Technol.*, 40 (3), 472–479.

[27] Yen, Ming-Tsung, Y., Joan-Hwa, Y., and Jeng-Leun, M., 2009, Physicochemical characterization of chitin and chitosan from crab shells, *Carbohydr. Polym.*, 75 (1), 15–21.

[28] Vaidyanathan, G., Sendhilnathan, S., and Arulmurugan, R., 2007, Structural and magnetic properties of $Co_{1-x}Zn_xFe_2O_4$ nanoparticles by co-precipitation method, *J. Magn. Magn. Mater.*, 313 (2), 293–299.

[29] López, J.A., González, F., Bonilla, F.A., Zambrano, G., and Gómez, M.E., 2010, Synthesis and characterization of Fe_3O_4 magnetic nanofluid, *Rev. Latinoam. Metal. Mater.*, 30 (1), 60–66.

[30] Vasile, E., Serafim, A., Dragusin, D.M., Petrea, C., Iovu, H., and Stancu, I.C., 2012, Apatite formation on active nanostructured coating based on functionalized gold nanoparticles, *J. Nanopart. Res.*, 14, 918.

[31] Biswas, S., Srivastava, V.K., and Ram, S., 2007, Nanorods of silver-coated magnetic CrO_2 particles from a polymer template in hot water, *J. Phys. Chem. C*, 111 (21), 7593–7598.

[32] Morales, M.P., Veintemillas-Verdaguer, S., Montero, M.I., Serna, C.J., Roig, A., Casas, L., Martinez, B., and Sandiumenge, F., 1999, Surface and internal spin canting in γ-Fe_2O_3 nanoparticles, *Chem. Mater.*, 11 (11), 3058–3064.

[33] Zhang, L., He, R., and Gu, H.C., 2006, Oleic acid coating on the monodisperse magnetite nanoparticles, *Appl. Surf. Sci.*, 253 (5), 2611–2617.

[34] Ho, K.M., and Li, P., 2008, Design and synthesis of novel magnetic core-shell polymeric particles, *Langmuir*, 24 (5), 1801–1807.

[35] Dung, D.T.K., Hai, T.H., Phuc, L.H., Long, B.D., Vinh, L.K., and Truc, P.N., 2009, Preparation and characterization of magnetic nanoparticles with chitosan coating, *J. Phys. Conf. Ser.*, 187, 012036.

[36] Tran, H.V., Tran, L.D., and Nguyen, T.N., 2010, Preparation of chitosan/magnetite composite beads and their application for removal of Pb(II) and Ni(II) from aqueous solution, *Mater. Sci. Eng., C*, 30 (2), 304–310.

[37] Pradhan, P., Giri, J., Samanta, G., Sarma, H.D., Mishra, K.P., Bellare, J., Banerjee, R., and Bahadur, D., 2006, Comparative evaluation of heating ability and biocompatibility of different ferrite-based magnetic fluids for hyperthermia application, *J. Biomed. Mater. Res. Part B*, 81 (1), 12–22.

[38] Jordan, A., Scholz, R., Wust, P., Fähling, H., and Felix, R., 1999, Magnetic fluid hyperthermia (MFH): Cancer treatment with AC magnetic field induced excitation of biocompatible superparamagnetic nanoparticles, *J. Magn. Magn. Mater.*, 201 (1-3), 413–419.

[39] Donadel, K., Felisberto, M.D.V., Fávere, V.T., Rigoni, M., Batistela, N.J., and Laranjeira, M.C.M., 2008, Synthesis and characterization of the iron oxide magnetic particles coated with chitosan biopolymer, *Mater. Sci. Eng.*, C, 28 (4), 509–514.